Structural, Electrical, Magnetic, and Spectroscopic Properties of Ring-Oxidized Molecular Metals Produced by Iodination of Metal-Free and Nickel Tetrabenzporphyrins

Kazuhiko Murata, Kwangkyoung Liou, Julia A. Thompson, Ellen M. McGhee, Dean E. Rende, Donald E. Ellis, Ronald L. Musselman,* Brian M. Hoffman,* and James A. Ibers*

Departments of Chemistry and Physics and Materials Research Center, Northwestern University, Evanston, Illinois 60208-3113, and Department of Chemistry, Franklin & Marshall College, Lancaster, Pennsylvania 17604-3003

Received December 13, 1996[⊗]

Detailed studies of the structure, conductivitity, magnetoresistance, optical spectra, and magnetic properties (susceptibility, EPR) for the new molecular metal tetrabenzporphyrin iodide (H_2(tbp)I) and the electrical, spectral, and magnetic properties of Ni(tbp)I are reported. Paramagnetic transition-ion impurities were carefully excluded during the synthesis of H_2(tbp)I and Ni(tbp)I, and both materials show much higher, metal-like conductivites than previously seen for less-pure Ni(tbp)I. Comparison of the specular reflectance data for Ni(tbp)I and H_2(tbp)I allows a distinction between purely ring π-transitions and metal-involved charge-transfer transitions, and the spectra fix the energy levels of the π orbitals involved in conduction. Transport, magnetic, and optical properties show that both H_2(tbp)I and Ni(tbp)I are ring-based conductors that have metal-like conductivities, varying as $\sim 1/T$, down to ca. 30−40 K. However, the remaining level of defects is higher in the tbp conductors than in H_2(pc)I, and whereas the latter is metallic down to the mK temperature range, the defects in the (tbp) compounds localize the conduction electrons at ~10 K (Ni(tbp)I) and ~30 K (H_2(tbp)I), leading to transport through one-dimensional variable-range hopping. EPR g-values for H_2(tbp)I and Ni(tbp)I are close to that for the free electron and are nearly temperature-independent. The line widths for both samples are extremely narrow and also are nearly temperature-independent. These results show that Ni(tbp)I does not display doubly-mixed valence, as thought earlier: Paramagnetic impurities significantly altered the EPR signals of the prior samples. H_2(tbp)I crystallizes in the space group $P4/mcc$ with cell constants of $a = 14.173(10)$ Å and $c = 6.463(4)$ Å. Full-matrix least-squares refinement of 63 variables gave an R index of 0.061 on F_o^2.

Introduction

We have extensively studied quasi one-dimensional molecular metals based on porphyrin molecules.[1−22] When the central metals and ligands are changed, the electrical, magnetic, and spectral properties are significantly modified. For example, negative thermoelectric power for Co(pc)I (pc = phthalocyanine) suggests that Co(pc)I is a metal-centered conductor where the Co d_{z^2} orbital is the path for conduction electrons.[23] In contrast, positive thermoelectric power for Co(tbp)I shows that oxidized tbp rings are the pathway for conduction electrons.[24] This is because it is easier to ring-oxidize (tbp) than (pc). We have also used single-crystal polarized reflectance spectroscopy to determine the energy levels of the π-orbitals involved with conduction in the macrocycle-based conductor. The lowest energy ligand-to-metal and metal-to-ligand charge-transfer transitions are dependent on the nature of the central metal and

* To whom correspondence should be addressed: R.L.M., Franklin & Marshall College; B.M.H. and J.A.I., Northwestern University.

[⊗] Abstract published in *Advance ACS Abstracts,* April 15, 1997.

(1) Hanack, M.; Roth, S.; Schier, H., Ed. *Proceedings of the International Conference on the Science and Technology of Synthetic Metals;* Elsevier Sequoia: Lausanne, Switzerland, 1991.
(2) Cowan, D. O.; Wiygul, F. M., *Chem. Eng. News* **1986**, *29*, 28−45.
(3) Ferraro, J. R.; Williams, J. M. In *Introduction to Synthetic Electrical Conductors;* Ed.; Academic Press: New York, 1987; pp 139−204.
(4) Williams, J. M.; Schultz, A. J.; Underhill, A. E.; Carneiro, K. In *Extended Linear Chain Compounds;* Miller, J. S., Ed.; Plenum Press: New York, 1982; pp 73−118.
(5) Miller, J. S.; Epstein, A. J. *Prog. Inorg. Chem.* **1976**, *20*, 1−151.
(6) Hoffman, B. M.; Ibers, J. A. *Acc. Chem. Res.* **1983**, *16*, 15−21.
(7) Marks, T. J. *Angew. Chem., Int. Ed. Engl.* **1990**, *29*, 857−879.
(8) Ogawa, M. Y.; Martinsen, J.; Palmer, S. M.; Stanton, J. L.; Tanaka, J.; Greene, R. L.; Hoffman, B. M.; Ibers, J. A. *J. Am. Chem. Soc.* **1987**, *109*, 1115−1121.
(9) Ogawa, M. Y.; Hoffman, B. M.; Lee, S.; Yudkowsky, M.; Halperin, W. P. *Phys. Rev. Lett.* **1986**, *57*, 1177−1180.
(10) Liou, K.; Ogawa, M. Y.; Newcomb, T. P.; Quirion, G.; Lee, M.; Poirier, M.; Halperin, W. P.; Hoffman, B. M.; Ibers, J. A. *Inorg. Chem.* **1989**, *28*, 3889−3896.
(11) Quirion, G.; Poirier, M.; Liou, K. K.; Ogawa, M. Y.; Hoffman, B. M.; Ibers, J. A. *Phys. Rev. B* **1988**, *37*, 4272−4275.
(12) Pace, L. J.; Martinsen, J.; Ulman, A.; Hoffman, B. M.; Ibers, J. A. *J. Am. Chem. Soc.* **1983**, *105*, 2612−2620.
(13) Liou, K. K.; Jacobsen, C. S.; Hoffman, B. M. *J. Am. Chem. Soc.* **1989**, *111*, 6616−6620.
(14) Ogawa, M. Y.; Palmer, S. M.; Liou, K. K.; Quirion, G.; Thompson, J. A.; Poirier, M.; Hoffman, B. M. *Phys. Rev. B* **1989**, *39*, 10682−10692.
(15) Quirion, G.; Poirier, M.; Liou, K. K.; Hoffman, B. M. *Phys. Rev. B: Condens. Matter* **1991**, *43*, 860−864.
(16) Godfrey, M. R.; Newcomb, T. P.; Hoffman, B. M.; Ibers, J. A. *J. Am. Chem. Soc.* **1990**, *112*, 7260−7269.
(17) Newcomb, T. P.; Godfrey, M. R.; Hoffman, B. M.; Ibers, J. A. *Inorg. Chem.* **1990**, *29*, 223−228.
(18) Newcomb, T. P.; Godfrey, M. R.; Hoffman, B. M.; Ibers, J. A. *J. Am. Chem. Soc.* **1989**, *111*, 7078−7084.
(19) Almeida, M.; Kanatzidis, M. G.; Tonge, L. M.; Marks, T. J.; Marcy, H. O.; McCarthy, W. J.; Kannewurf, C. R. *Solid State Commun.* **1987**, *63*, 457−461.
(20) Yakushi, K.; Yamakado, H.; Ida, T.; Ugawa, A. *Solid State Commun.* **1991**, *78*, 919−923.
(21) Yakushi, K.; Sakuda, M.; Hamada, I.; Kuroda, H.; Kawamoto, A.; Tanaka, J.; Sugano, T.; Kinoshita, M. *Synth. Met.* **1987**, *19*, 769−774.
(22) Yakushi, K.; Ida, T.; Ugawa, A.; Yamakado, H.; Ishii, H.; Kuroda, H. *J. Phys. Chem.* **1991**, *95*, 7636−7641.
(23) Martinsen, J.; Stanton, J. L.; Greene, R. L.; Tanaka, J.; Hoffman, B. M.; Ibers, J. A. *J. Am. Chem. Soc.* **1985**, *107*, 6915−6920.
(24) Liou, K. Y.; Newcomb, T. P.; Heagy, M. D.; Thompson, J. A.; Heuer, W. B.; Musselman, R. L.; Jacobsen, C. S.; Hoffman, B. M.; Ibers, J. A. *Inorg. Chem.* **1992**, *31*, 4517−4523.

S0020-1669(96)01490-5 CCC: $14.00

the identity of the macrocycle.[25,26] In particular for Co, the p^{π} orbitals are higher in energy for Co(tbp)I than for Co(pc)I[24] and the HOMO for the former is a p^{π} orbital not the metal d_{z^2} orbital. Thus Co(tbp)I is a ring conductor as are the Ni(pc)I and Cu(pc)I, rather than a metal-spine conductor as is Co(pc)I. Recent calculations that compared Ni(tbp)I with several M(pc)I compounds[27] predict that the p^{π} levels should be *lower* in Ni(tbp)I than in Ni(pc)I, raising the possibility that they may be below the metal d_{z^2} level and that Ni(tbp)I will be a metal-spine conductor.

We have recently found that electrical and magnetic properties of porphyrinic molecular metals are far more sensitive to organic impurities, structural defects, and paramagnetic metal centers than we had appreciated.[28] In order to remove as many of these factors as possible, we revisited an early system, the phthalocyanines (pc's), obtaining much higher purity H_2(pc)I and Ni(pc)I. The maximum conductivity for single crystals of these samples is about 5−6 times larger than for those reported previously.[29−32] These "clean" background conductors enabled us to study the effect of impurities on the electrical and magnetic properties.[33] Organic impurities and structural defects act as sources of random potential and lead to a localized electronic state.[34−36] Electrical conductivity is reduced in the localized state and is limited by variable-range hopping.[37−39] Paramagnetic metal impurities, such as Cu^{II}, Co^{II}, and Fe^{II}, also reduce the conductivity of porphyrinic molecular metals but by a different mechanism known as the Kondo effect.[40−43]

We report here structural, electrical, UV−vis polarized specular reflectance, and magnetic properties of the new molecular metal H_2(tbp)I, prepared in a manner similar to the purer pc's in order to avoid the contamination of paramagnetic impurities. We also report a restudy of electrical and magnetic properties for a sample of Ni(tbp)I having a much lower level of paramagnetic impurities than before.[44,45] Comparison of the specular reflectance data for Ni(tbp)I and H_2(tbp)I allows a distinction between purely ring π-transitions and metal-involved charge-transfer (CT) transitions, and the spectra fix the energy levels of the π-orbitals involved in conduction. Transport, magnetic, and optical properties show that both H_2(tbp)I and Ni(tbp)I are ring-based conductors, and they exhibit high, metal-like conductivities down to ca. 30−40 K. However, the remaining level of defects is higher than in H_2(pc)I, and whereas the latter is metallic down to the mK temperature range, the defects in the (tbp) compounds localize the conduction electrons at low temperatures, leading to transport through one-dimensional variable-range hopping.[46] Ni(tbp)I does not show doubly-mixed valence, as thought earlier, where both Ni d_{z^2} orbitals and tbp rings are oxidized owing to the hopping of the conduction electrons between the d_{z^2} orbitals and the rings:[44] Paramagnetic impurities had significantly altered the EPR signals of the prior samples.

Experimental Section

Zn(tbp). Zinc acetate dihydrate was prepared from ultrapure zinc shot (Johnson Matthey, 99.9999%) and freshly distilled acetic acid. Zn(tbp) was synthesized by the template cyclization of isoindolinone-3-acetic acid with zinc acetate dihydrate by utilizing the method of Edwards *et al.*[47] but excluding the purification process. Zn(tbp) was extracted from the reaction mixture with pyridine and recrystallized from 1-chloronaphthalene until the impurity peak appearing at 460 nm in the optical spectrum was removed.

H_2(tbp). Metal-free tetrabenzporphyrin was obtained by the demetalation of Zn(tbp) in cold concentrated sulfuric acid saturated with hydrogen chloride gas. The sulfuric acid solution of Zn(tbp) was poured onto ice in order to avoid the sulfonation of the tbp rings. The resulting precipitate was washed with cold water and dried before extraction with 1-chloronaphthalene with the use of a quartz Linstead hot-extraction apparatus[48] and a high-purity glass thimble (Whatman). The material obtained after cooling the solution had a blue-purple luster, and its optical solution spectrum showed no trace of Zn(tbp). H_2(tbp) was further purified by sublimation under vacuum (less than 10^{-3} Torr) at 450 °C. The overall yield was 7.9% from isoindolinone-3-acetic acid.

Ni(tbp). H_2(tbp) was metalated with twice the stoichiometric amount of 99.9985% $NiCl_2 \cdot 6H_2O$ (Johnson Matthey) in a 10% quinoline/1-chloronaphthalene solvent. The solution was refluxed in a fused-silica vessel for 72 h and then cooled in an ice bath. The dark-purple Ni(tbp) crystals that precipitated were removed by filtration and washed with hot water and acetone. The progress of the metalation was followed by UV−vis solution spectroscopy, and the reaction was repeated until the peak at 666 nm in the UV−vis spectrum associated with H_2(tbp) was removed. The resulting Ni(tbp) was sublimed twice in vacuum at 450 °C. The yield from H_2(tbp) was 91%.

H_2(tbp)I and Ni(tbp)I. Single crystals of H_2(tbp)I and Ni(tbp)I were grown by oxidizing H_2(tbp) and Ni(tbp), respectively, with a 20% molar excess of I_2 in 1-chloronaphthalene at *ca.* 200 °C in shielded fused-silica H-tubes. A higher temperature is needed to dissolve tbp as opposed to pc. The silica tubes have an extra horizontal tube to equalize the level of the solvent. If too much iodine is used, then tbp is overoxidized. Shiny dark-green crystals of H_2(tbp)I and Ni(tbp)I were collected by filtration. Anal. Calcd for $C_{36}H_{22}IN_4$: C, 67.8; H, 3.49; N, 8.78. Found: C, 69.0; H, 3.49; N, 8.68. Calcd for $C_{36}H_{20}IN_4Ni$: C, 62.28; H, 2.91; N, 8.07. Found: C, 62.07; H, 2.78; N, 8.13 (Nippon Shokubai Central Research Laboratory, Osaka, Japan).

X-ray Diffraction Study of H_2(tbp)I. From Weissenberg X-ray photographs, we assigned the H_2(tbp)I crystals to Laue group 4/*mmm* of the tetragonal system. Systematic absences are consistent with the space groups *P*4/*mcc* and *P*4*cc*. Agreement among Friedel pairs (R_{int}

(25) Heagy, M. D.; Rende, D. E.; Shaffer, G. W.; Wolfe, B. M.; Liou, K.; Hoffman, B. M.; Musselman, R. L. *Inorg. Chem.* **1989**, *28*, 283−286.
(26) Rende, D. E.; Heagy, M. D.; Heuer, W. M.; Liou, K.; Thompson, J. A.; Hoffman, B. M.; Musselman, R. L. *Inorg. Chem.* **1992**, *31*, 352−358.
(27) Liang, X.; Flores, S.; Ellis, D. E.; Hoffman, B. M.; Musselman, R. L. *J. Chem. Phys.* **1991**, *95*, 403−417.
(28) Thompson, J. A.; Murata, K.; Miller, D. C.; Stanton, J. L.; Broderick, W. E.; Hoffman, B. M.; Ibers, J. A. *Inorg. Chem.* **1993**, *32*, 3546−3553.
(29) Schramm, C. J.; Scaringe, R. P.; Stojakovic, D. R.; Hoffman, B. M.; Ibers, J. A.; Marks, T. J. *J. Am. Chem. Soc.* **1980**, *102*, 6702−6713.
(30) Martinsen, J.; Greene, R. L.; Palmer, S. M.; Hoffman, B. M. *J. Am. Chem. Soc.* **1983**, *105*, 677−678.
(31) Martinsen, J.; Palmer, S. M.; Tanaka, J.; Greene, R. C.; Hoffman, B. M. *Phys. Rev. B* **1984**, *30*, 6269−6276.
(32) Inabe, T.; Marks, T. J.; Burton, R. L.; Lyding, J. W.; McCarthy, W. J.; Kannewurf, C. R.; Reisner, G. M.; Herbstein, F. H. *Solid State Commun.* **1985**, *54*, 501−504.
(33) Murata, K.; Ohashi, Y.; Murata, K.; Thompson, J. A.; Mori, M.; Hoffman, B. M. *Synth. Met.* **1993**, *56*, 1777−1782.
(34) Lee, P. A. *Rev. Mod. Phys.* **1985**, *57*, 287−337.
(35) Nagaoka, Y. *Prog. Theor. Phys. Suppl.* **1985**, *84*, 1−15.
(36) Anderson, P. W. *Science* **1978**, *201*, 307−316.
(37) Mott, N. F. *Metal-Insulator Transitions*, 2nd ed.; Taylor & Francis: London, 1990.
(38) Mott, N. F.; Kaveh, M. *Adv. Phys.* **1985**, *34*, 329−401.
(39) Ambegaoker, V.; Halperin, B.; Langer, J. S. *Phys. Rev.* **1971**, *4*, 2612−2620.
(40) Kondo, J. *Prog. Theor. Phys.* **1964**, *32*, 37−49.
(41) Gruner, G.; Zawadowski, A. *Rep. Prog. Phys.* **1974**, *37*, 1497−1583.
(42) Kondo, J. In *Solid State Physics;* Seitz, F., Turnbull, D., Ehrenreich, H., Ed.; Academic Press: New York, 1969; pp 183−281.
(43) Brandt, N. B.; Moshchalkov, V. V. *Adv. Phys.* **1984**, *33*, 373−468.
(44) Martinsen, J.; Pace, L. J.; Phillips, T. E.; Hoffman, B. M.; Ibers, J. A. *J. Am. Chem. Soc.* **1982**, *104*, 83−91.
(45) Euler, W. B.; Martinsen, J.; Pace, L. J.; Hoffman, B. M.; Ibers, J. A. *Mol. Cryst. Liq. Cryst.* **1982**, *81*, 231−242.
(46) Bloch, A. N.; Weisman, R. B.; Varma, C. M. *Phys. Rev. Lett.* **1972**, *28*, 753−756.
(47) Edwards, L.; Weisman, R. B.; Varma, C. M. *Phys. Rev. Lett.* **1972**, *28*, 7638−7641.
(48) Barrett, P. A.; Dent, C. E.; Linstead, R. P. *J. Chem. Soc.* **1936**, 1719−1736.

Table 1. Crystal Data and Experimental Details for H_2(tbp)I

compd	tetrabenzoporphyrin iodide
formula	$C_{36}H_{22}N_4I$
fw	637.51
a, Å	14.173(10)
c, Å	6.463(4)
V, Å^3	1298
Z	2
d_{calc}, g cm^{-3}	1.631(3)
space group	D_{4h}^2-*P*4/*mcc*
μ, cm^{-1}	12.5
transm coeff	0.826−0.851
R on F_o^2	0.061
R_w on F_o^2	0.104
R on F_o with $F_o^2 > 3\sigma(F_o^2)$	0.039

= 0.025 after correction for absorption) and successful refinement of the structure support the choice of space group D_{4h}^2-*P*4/*mcc*. Least-squares refinement of 14 reflections centered on a Picker diffractometer yielded cell constants of $a = 14.173(10)$ Å and $c = 6.463(4)$ Å (λ(Mo Kα_1) = 0.7093 Å). In addition to the normal Bragg scattering, diffuse scattering was observed, similar to that found in the Ni(tbp)I and Ni(pc)I systems.[29,44] The diffuse scattering, observable on oscillation photographs, was found in planes perpendicular to the c^* axis with a spacing of $c^{*\prime} = {}^2/_3c^*$. No diffuse layers with $l' = 3n$ were observed.

The data for the Bragg scattering were collected at 123 K with the $\theta-2\theta$ scan technique. No systematic changes were seen in the six standard reflections that were measured every 100 reflections. The final refinement on F_o^2 converged to $R(F_o^2) = 0.061$ for 999 observations and 63 variables.[49] In this refinement the positions of the hydrogen atoms were idealized (C−H = 0.95 Å) and each hydrogen atom was given an isotropic thermal parameter 1 Å^2 larger than that of the carbon atom to which it is bonded. Experimental details and crystal data are found in Table 1. Other crystallographic details are in the Supporting Information.

Intensity data for the diffuse scattering were collected at 123 K point by point along a line perpendicular to the diffuse planes. Two data sets were collected: (1) every 0.05° in 2θ with a counting time of 100 s per step; (2) every 0.10° in 2θ with a counting time of 200 s per step. The data were collected out to $l' = 11$. The $l' = 1$ peak was not discernible from the background. The two different data sets were averaged and corrected for absorption and Lorentz−polarization effects.

As in Ni(tbp)I, the apparent thermal parameter of the iodine atom was larger along the chain ($U_{||} = 0.0957(5)$ Å^2). The diffuse lines may be ascribed to the disorder in the iodine chains that leads to this anomalous thermal motion. A reasonable model that accounts for this disorder[29] proposes that there are ordered chains of symmetric I_3^- ions with repeat distance $c' = 3c/2$ but that the origins of these chains are out of register. This lack of register gives rise to the observed diffuse scattering. From an analysis of that scattering, we can obtain the value of *d*, the displacement parameter, and hence the I−I distance in the I_3^- ion. A least-squares fit to the previously derived expression[29,50]

$$|F_d(l)|^2 = (1/9)[(1 + 2\cos[2\pi l(d - {}^1/_3)])^2][9 - (1 + 2\cos[2\pi l/3])^2] \quad (1)$$

yields $d = 0.0213(1)$. The observed and calculated values of the diffuse structure amplitudes (Supporting Information) lead to an *R* index for these intensities of 0.088.

Single-Crystal Electrical Conductivity Studies. Single crystals of both H_2(tbp)I and Ni(tbp)I were mounted on graphite fibers with a locally prepared palladium paste. Four-probe ac (27 Hz) conductivity measurements were performed along the stacking axis. A Stanford Research SR-530 two-channel lock-in amplifier was used to measure the voltage drop across the sample in the differential mode. A Quantum Design SQUID susceptometer was used to apply a transverse field up to 5 T and to control the temperature between 300 and 1.85 K. All crystals showed ohmic properties for the current between 10^{-6} and 10^{-3} A.

Single-Crystal Polarized Reflectance Spectroscopy. Polarized specular reflectance spectra were obtained with an instrument described in detail elsewhere.[51] Spectra were recorded from elongated faces ((100) and (010)) of both H_2(tbp)I and Ni(tbp)I with the electric vector aligned either parallel or perpendicular to the needle (*c*) axis of the crystals. Since the macrocycle planes are aligned perpendicular to the *c* axis (see below), parallel and perpendicular to the needle axis correspond to out of plane and in plane, respectively. For each spectrum 400 data points were collected between 215 and 850 nm. Collection at each data point for each individual spectrum proceeded until the sample mean had a 99% probability of being within 1% of the population mean. For each sample, three or four individual spectra were averaged once the data were corrected for percent reflectivity relative to a NIST standard mirror. For Kramers−Kronig analysis,[52,53] reflectivities beyond our experimental region were estimated in the infrared region from values for Ni(pc)I and Co(pc)I[23,31] and were approximated in the vacuum ultraviolet and beyond so as to produce baselines approaching zero absorbance in regions known to have no absorbance in related systems in the vapor state. Deconvolution was carried out with an interactive Gaussian and Lorentzian program ("FastGauss"[54]).

Electron Paramagnetic Resonance Measurements. Measurements at room temperature and 77 K were carried out with the use of a modified Varian E-4 X-band ESR spectrometer. Data recorded between 1.8 and 4.2 K were taken on powdered samples with a modified Varian E-109 Q-band ESR spectrometer for H_2(tbp)I or a Bruker ER 200D-SRC X-band ESR spectrometer for Ni(tbp)I. Experiments were performed with a silvered TE102 sample cavity in a Janis Corp. liquid-helium immersion Dewar flask. The temperature was regulated by controlling the He pressure inside the Dewar. For the calibration of the field, 2,2-phenyl-1-picrylhydrazyl (DPPH), recrystallized from benzene ($g = 2.0036$ at 300 K, $g = 2.0025$ at 4.2 K), was used. Computer simulations of the powder patterns generated by the program Qpow[55−57] were used to determine *g*-values and line widths.

Magnetic Susceptibility Measurements. Static magnetic susceptibility measurements were taken from 300 to 1.9 K with a Quantum Design SQUID susceptometer. Gelatin capsules were used to hold the samples, and the background was measured over the full temperature range just prior to measuring the sample. Data were recorded at 5 kG on 20−40 mg samples.

Results and Discussion

Structure of H_2(tbp)I. Not surprisingly, the structure of H_2(tbp)I is very similar to that of Ni(tbp)I.[44] The macrocycles are stacked in chains that run parallel to the *c* axis, with chains of iodine atoms in the channels between the stacks. The two H_2(tbp) molecules within the unit cell are staggered by 40°. The porphyrin macrocycles are necessarily planar because they lie upon sites of 4/*m* symmetry. Figure 1 is a perspective drawing of the H_2(tbp) molecule. The thermal parameter of the iodine atom in the stacking direction is much larger than that perpendicular to the stack. This evidence supports the disordered I_3^- model[29] for H_2(tbp)I.

The molecular structure is similar to that of Ni(tbp)I, but there are some notable differences (Supporting Information). Replacement of the Ni center with protons causes the coordinating pyrrole nitrogen atoms to move away from the center of the ring. Thus, the angles around the nitrogen atoms are larger in H_2(tbp)I than in Ni(tbp)I, and the central hole of the macrocycle is expanded.

(49) $R(F_o^2) = \Sigma|F_o^2 - F_c^2|/\Sigma F_o^2$.

(50) Guinier, A. *X-Ray Diffraction in Crystals, Imperfect Crystals and Amorphous Bodies;* W. H. Freeman: San Francisco, CA, 1963.
(51) Desjardins, S. R.; Penfield, K. W.; Cohen, S. L.; Musselman, R. L.; Solomon, E. I. *J. Am. Chem. Soc.* **1983**, *105*, 4590.
(52) Anex, B. G. *Mol. Cryst.* **1966**, *1*, 1−36.
(53) Kronig, R. *J. Opt. Soc. Am.* **1926**, *12*, 547.
(54) Haddon, H.; Musselman, R. L. FastGauss, Macintosh Application, Franklin and Marshall College, 1992.
(55) Belford, R. L.; Nilges, M. J., Eds. In *Computer Simulation of Powder Spectra;* EPR Symposium, 21st Rocky Mountain Conference, Denver, CO, 1979.
(56) Nilges, M. J. Ph.D. Dissertation, University of Illinois, 1979.
(57) Maurice, A. M. Ph.D. Dissertation, University of Illinois, 1980.

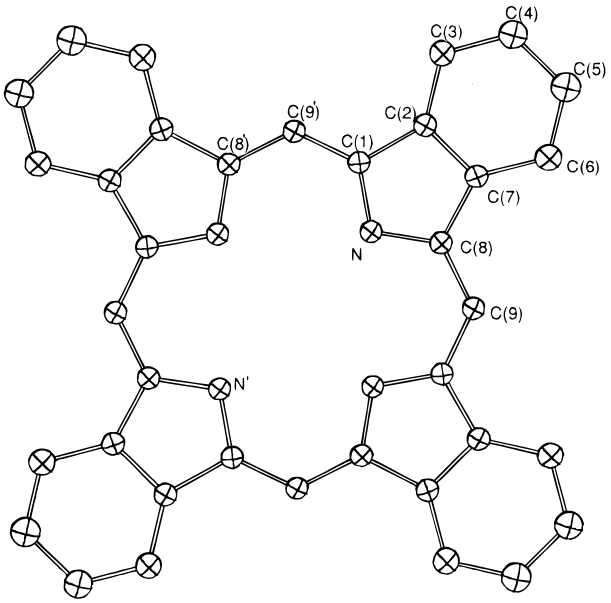

Figure 1. Perspective view of the tbp macrocycle, hydrogen atoms omitted.

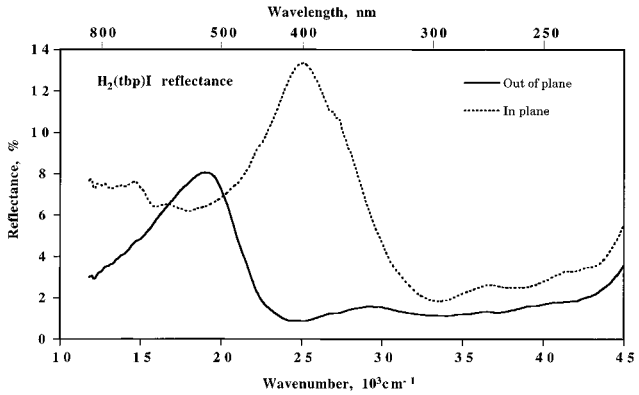

Figure 2. Polarized specular reflectance spectra of a single crystal of H_2(tbp)I: — = electric vector perpendicular to (out of plane) and --- = parallel to (in plane) molecular planes.

Single-Crystal Reflectance Spectroscopy. Specular reflectance spectroscopy was used to obtain polarizations of electronic transitions, since the high absorbances made transmission spectroscopy impractical. Comparison of the spectra of Ni(tbp)I and H_2(tbp)I is helpful in distinguishing metal-involved CT transitions from purely ring π-transitions. There is a complication from three out-of-plane I_3^- transitions, one of which falls in the region of the lowest energy MLCT band, the $d_{z^2} \rightarrow \pi,p_z$ transition in M(pc)I [25,26] and Co(tbp)I;[24] the low-energy out-of-plane-polarized transitions can be differentiated with the help of spectra from H_2(tbp)I.

H_2(tbp)I. We show the reflectance spectra of H_2(tbp)I in Figure 2 and the Kramers−Kronig-transformed absorbance spectra in Figure 3a,b. The transformed spectrum with the electric vector parallel to the *c* axis and out of the complex plane is shown in Figure 3b. As with all peaks in this compound and in Ni(tbp)I, Gaussian deconvolution gave a better fit for well-defined peaks than did Lorentzian deconvolution and was thus used. The lowest energy out-of-plane peaks, D−F in Figure 3b, match very closely the corresponding peaks in H_2(pc)I,[26] all of which were assigned as arising from I_3^-, the actual form of the reduced I species in the crystal. We thus assign these three peaks as we did their counterparts in H_2(pc)I: peak D at 19.95×10^3 cm^{-1} as the $^1S_g \rightarrow {}^1S_u$* transition, peak F at 30.4 $\times 10^3$ cm^{-1} as a spin−orbit component of peak D, and peak E

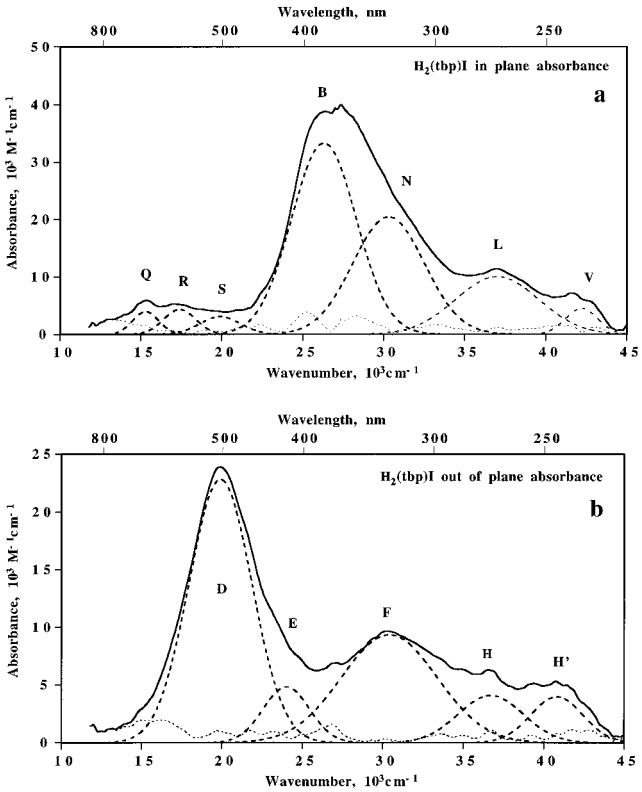

Figure 3. Absorbance spectra of H_2(tbp)I from Kramers−Kronig-transformed reflectance data: (a, top) in-plane polarized; (b, bottom) out of plane polarized; —, experimental data; ---, Gaussian deconvolution; ···, residual.

at 24×10^3 cm^{-1} as a transition from I_3^- only in the solid state. Peaks H and H′ are similar to two relatively low-intensity, high-energy peaks in H_2(pc)I; neither of these peaks is predicted in recent theoretical treatments,[27,58] and these remain unassigned. The in-plane spectrum for H_2(tbp)I, Figure 3a, shows a Soret region, peak B, and a greatly reduced Q band relative to that in H_2(pc)I,[26] consistent with porphyrin Q bands being much lower in intensity relative to the Soret band than the phthalocyanine Q bands.[59] This spectrum is remarkably similar to the in-plane spectrum for Co(tbp)I,[24] and we assign the transitions as we did in that system: Q at 15.3×10^3 cm^{-1} as $2a_{1u}(\pi) \rightarrow 7e_g(\pi^*)$ and R at 17.4×10^3 cm^{-1} as $5a_{1u}(\pi) \rightarrow 7e_g(\pi^*)$. These two transitions are calculated to be at 15 136 and 20 7120 cm^{-1} for Ni(tbp)I.[27]

The intense peak in Figure 3a at 26 300 cm^{-1} corresponds to the Soret band in solution spectra of porphyrins. We recently assigned this band in M(pc)I systems[26,27] and in Co(tbp)I to be primarily $6e_g(\pi) \rightarrow 4b_{2u}(\pi^*)$ with minor contributions from several much weaker transitions. Our calculations on Ni(tbp)I[27] show several transitions around 27 000 cm^{-1}, the strongest being $6e_g(\pi) \rightarrow 4b_{2u}(\pi^*)$. Others include $2b_{1u} \rightarrow 7e_g$ and $4a_{2u} \rightarrow 7e_g$. We thus assign peak B as primarily $6e_g(\pi) \rightarrow 4b_{2u}(\pi^*)$ with minor contributions from $2b_{1u}(\pi) \rightarrow 7e_g(\pi^*)$ and $4a_{2u}(\pi) \rightarrow 7e_g(\pi^*)$. Note that this assignment differs from that of the four-orbital model,[60,61] where the Soret transition has been assigned as $4a_{1u}(\pi) \rightarrow 6e_g(\pi^*)$, equivalent to the $5a_{1u}(\pi) \rightarrow 7e_g(\pi^*)$ that we assign to peak R. The structure at the top of peak B we attribute to instrument noise since it falls within the background

(58) Liang, X. L.; Ellis, D. E.; Gubanova, O. V.; Hoffman, B. M.; Musselman, R. L. *Int. J. Quantum Chem.* **1994**, *52*, 657−671.
(59) Schaffer, A. M.; Gouterman, M.; Davidson, E. R. *Theoret. Chim. Acta* **1973**, *30*, 9.
(60) Edwards, L.; Gouterman, M. *J. Mol. Spectrosc.* **1970**, *33*, 292.
(61) Basu, S. *Ind. J. Phys.* **1955**, *28*, 511.

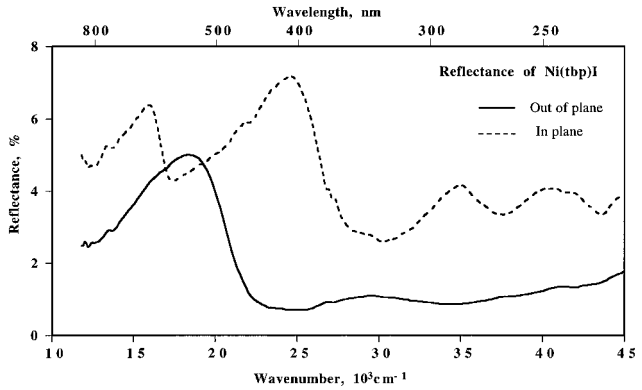

Figure 4. Polarized specular reflectance spectra of a single crystal of Ni(tbp)I: —, out of plane; ---, in plane.

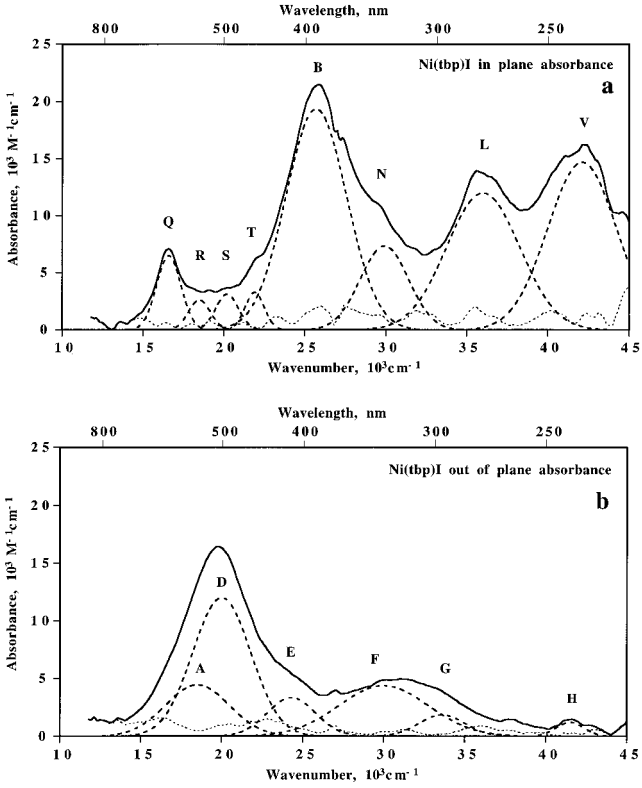

Figure 5. Absorbance spectra of Ni(tbp)I from Kramers−Kronig-transformed reflectance data: (a, top) in-plane polarized; (b, bottom) out of plane polarized; —, experimental data; ---, Gaussian deconvolution; ···, residual.

signals in the deconvolution. The remaining peaks N, L, and V fall in the region where at least five moderately intense ($0.14 \leq f \leq 0.51$) transitions are predicted for Ni(tbp)I: $6e_g \rightarrow 3b_{1u}$, $6e_g \rightarrow 6a_{2u}$, $5e_g \rightarrow 3b_{1u}$, $2a_{1u} \rightarrow 9e_g$, and $2b_{1u} \rightarrow 8e_g$. Presumably these five transitions contribute to much of the intensity in this region. The labels are chosen to be consistent with earlier treatments of porphyrin spectra.[26,60]

Ni(tbp)I. The reflectance spectra of Ni(tbp)I are shown in Figure 4, and the transformed absorbance spectra are shown in Figure 5a,b. The in-plane spectrum (Figure 5a) is essentially identical to that for H_2(tbp)I (Figure 3a), and as noted above, our calculations for the Ni(tbp)I spectra agree with the experimental in-plane peaks. We will therefore assign peaks Q, R, S, B, N, L, and V to the same transitions as in H_2(tbp)I. Peak T is not predicted in our calculations and likely arises from a monochromator aberration at 22 000 cm^{-1}.

The out-of-plane spectra of Figure 5b contain the first metal-related information in this set, but we first need to identify the peaks from I_3^-. Peaks D−F have been identified as arising from a $^1\Sigma_g \rightarrow {}^1\Sigma_u^*$ transition, a spin−orbit coupling component, and a solid-state induced component, respectively. These peaks also appear in Figure 5b, but the Gaussian deconvolution needs to be described because of the close proximity of the I_3^- and Ni(tbp)I CT peaks. Peaks D and F have appeared within 400 cm^{-1} of 20 000 and 30 000 cm^{-1}, respectively, in both H_2(pc)I[26] and H_2(tbp)I, and it is reasonable to assume that their positions will not change in Ni(tbp)I since the environment of I_3^- anion is similar in all three compounds. It is also reasonable to assume that the relative integrated intensities will remain nearly constant in all three compounds. The reliability of intensity data is the principal limitation of our specular reflectance measurements. Both inaccuracies in the raw intensities and inherent uncertainties in the reflectance data beyond our experimental region affect the intensities. The practice of estimating far UV reflectance with an "effective reflectance" is essentially sound.[52] Although the energies of peaks are unaffected by uncertainties in unobservable reflectances, the slope of the transformed absorbance baseline, necessary for the estimation of relative intensities, is principally affected by changes in the shape of the effective reflectance. Table 2 lists several characteristics of the I_3^- transitions in H_2(pc)I and H_2(tbp)I, as well as the results arrived at for Ni(tbp)I from these intensity and energy considerations. The ratio of q^2 for peaks D:F is 3.54 in H_2(pc)I and 2.44 in H_2(tbp)I. If no allowance were made for peaks A and G in Ni(tbp)I, this same ratio would have the value 1.31. When we place peak F at 30 000 cm^{-1} and target an intensity ratio between 3.5 and 2.4 to obtain the adjusted peaks D and F listed in Table 2, we obtain a q^2 ratio of 2.66. The estimated deconvoluted peaks A and G that result from this adjustment are shown in Figure 5b.

Table 2. I_3^--Based UV−Vis Peaks

compd	peak	wavenumber at max abs (10^{-3} cm^{-1})	max abs (10^3 M^{-1} cm^{-1})	intensity, q^2 (Å^2)
H_2(pc)I	D	19.65	22.848	4.6
	E	23.95	4.61	3.3
	F	29.95	5.97	6.2
H_2(tbp)I	D	19.95	22.85	4.6
	E	24	4.85	3.4
	F	30.4	9.36	7
Ni(tbp)I	D	20	12	4.2
	E	24.35	3.34	3.5
	F	30.05	4.38	6.5

Peak A at 18 550 cm^{-1} is analogous to $a_{1g}(d_{z^2}) \rightarrow a_{2u}(p_z,\pi^*)$ transitions found in Co(pc)I, Ni(pc)I,[25] Cu(pc)I,[26] and Co(tbp)I.[24] The energies of the M(pc)I $a_{1g}(d_{z^2}) \rightarrow a_{2u}(p_z,\pi^*)$ transitions are 14.5, 18.4, and 18.8 × 10^3 cm^{-1}, respectively, following the expected energies of metal orbitals. The energy of the same transition in Co(tbp)I is 18 000 cm^{-1}, a blue shift of 3500 cm^{-1} from that in Co(pc)I. This was interpreted[24] as resulting from a larger central cavity for tbp, causing a drop in the d_{z^2} orbital and a rise in the π^* orbitals in tbp owing to the less electronegative methylene carbon atoms in the pyrole-bridging positions. In the present case of Ni(tbp)I there is only a slight blue shift of 150 cm^{-1}. The end result is that the $a_{1g}(d_{z^2}) \rightarrow a_{2u}(p_z,\pi^*)$ transition in Ni(tbp)I is 550 cm^{-1} higher than that in Co(tbp)I, consistent with parallel results in M(pc)I compounds. Nevertheless, from the comparison between the $a_{1g}(d_{z^2}) \rightarrow a_{2u}(p_z,\pi^*)$ transitions in Co(tbp)I and Ni(tbp)I we conclude that the Ni $3d_{z^2}$ orbital lies below that of Co and hence that partial oxidation occurs on the macrocycle ring.

Electrical Conductivity. The single-crystal electrical conductivity along the stacking axis at room temperature is in the range of 300−1200 S cm^{-1} for both H_2(tbp)I and Ni(tbp)I. The

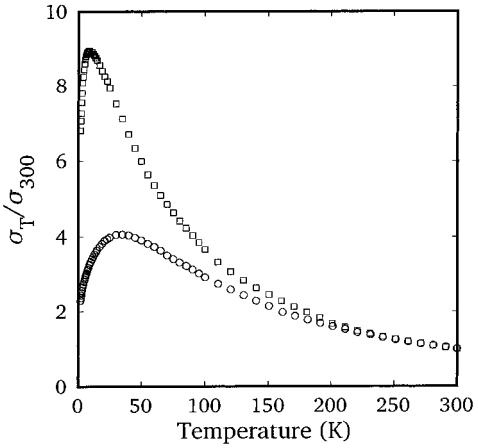

Figure 6. Single-crystal conductivity as a function of temperature for H_2(tbp)I (○) and Ni(tbp)I (□).

broad range arises from uncertainties in the size of the crystals. The conductivity normalized to that at room temperature, however, is reproducible; it is shown in Figure 6 as a function of temperature for both H_2(tbp)I and Ni(tbp)I. The conductivities show similar temperature dependences. With decreasing temperature, the conductivities increase as do metals ($d\sigma/dT < 0$), reach a local maximum, and then decrease as semiconductors do ($d\sigma/dT > 0$). The maximum normalized conductivity ($\sigma_{max}/\sigma_{300}$) is 4.1 at 35 K for H_2(tbp)I and is 8.9 at 9 K for Ni(tbp)I. The conductivity ratios at 1.85 K are 2.3 and 6.8 for H_2(tbp)I and Ni(tbp)I, respectively. The maximum conductivity of Ni(tbp)I reported here is much higher than that reported previously ($\sigma_{max}/\sigma_{300} = 1.8$ at 95 K), and it occurs at a lower temperature (T_{max}(K)). This major improvement in the conductivity of Ni(tbp)I is brought about by the decreased level of impurities, especially of paramagnetic metals, such as Cu^{II}, Co^{II}, and Fe^{II}. Only a trace (<50 ppm) of Cu(tbp)I was detected by EPR measurements on H_2(tbp)I and Ni(tbp)I. Note that Ni^{II} is diamagnetic in square-planar coordination.

The increase in conductivity with decreasing temperature results from the reduction of phonon scattering found in typical metals. The temperature dependence of the conductivity below T_{max} shows variable-range hopping. For one-dimensional conductors, the conductivity follows the equation, $\sigma \propto \exp(T_0/T)^{-1/2}$, where T_0(K) is a parameter close to T_{max}. The conductivities of both H_2(tbp)I and Ni(tbp) below T_{max} are limited by such hopping. The combination of the two contributions, phonon scattering that dominates at high temperatures and variable-range hopping that dominates at low temperatures, results in the conductivity maximum. Because of variable-range hopping the conduction electrons are localized at low temperatures. We recently reported that the conductivity of Ni(pc)I increases as the defects in pc rings are reduced; the defects are the source of random potential that causes a localized electronic state.[28] Similar arguments could be made for H_2(tbp)I and Ni(tbp)I where the crystal defects in tbp rings localize the conduction electrons at low temperatures. But owing to the limitations in the respective synthetic routes (see above) it has not been possible to reduce crystal defects in tbp as much as they can be in pc. Although the conducting behavior for Ni(pc)I is very similar to that for H_2(pc)I, the conductivity for Ni(tbp)I is higher than that for H_2(tbp)I because Ni(tbp)I contains fewer impurities.

Magnetoresistance ($\Delta/\rho_0 = (\rho_H - \rho_0)/\rho_0$) at 1.85 K is plotted as a function H^2, the square of the magnetic field, for H_2(tbp)I and Ni(tbp)I in Figure 7. Both H_2(tbp)I and Ni(tbp)I show similar behavior. The data for Ni(tbp)I are noisy because a single crystal of Ni(tbp)I is extremely fragile; this behavior

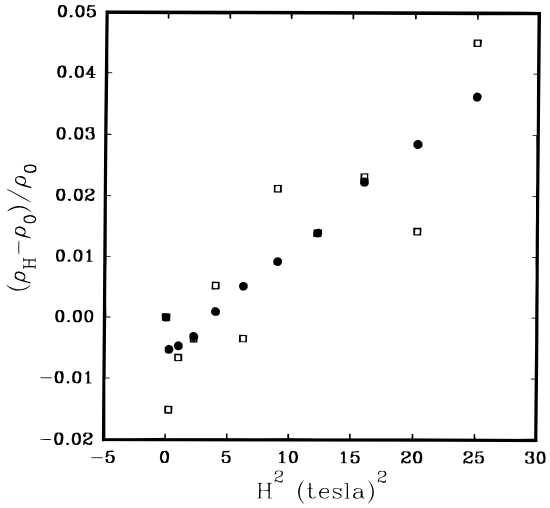

Figure 7. Magnetoresistance, $(\rho_H - \rho_0)/\rho$, as a function of the square of the magnetic field, H^2: H_2(tbp)I (●); Ni(tbp)I (□).

should not be attributed to a Schubnikov−deHaas oscillation. As shown in Figure 7 the magnetoresistance is linear with H^2, being negative at low fields and becoming positive at high fields. The magnetoresistance can be interpreted as the sum of a negative term that tends to saturate with increasing field and a positive term that does not saturate. The negative contribution is explained by the Kondo effect.[37−39] Because of the trace (<50 ppm) of Cu(tbp)I impurity, the conduction electrons are scattered at low temperatures by the local moments in Cu^{II} $d_{x^2-y^2}$ orbitals. In a magnetic field the direction of the local spins is frozen and s−d exchange interaction between conduction electrons and local spins is prevented. As a result the resistivity in the magnetic field decreases. Positive quadratic magnetoresistance is observed in many atomic metals. Such quadratic dependence is explained by the drift velocity model that considers two types of carriers, for example electrons and holes.[62] Negative magnetoresistance, explained by a change of Fermi energy owing to the Zeeman effect, is often observed for localized electronic systems.[63] But this would not lead to the magnitude of the negative magnetoresistance being related to the amount of paramagnetic impurities, as is found here. The positive effect is also expected in localized systems with electron−electron interactions.[64] But this does not apply here as the magnitude of the positive magnetoresistance is not related to the magnitude of localization.

Magnetic Susceptibility. The variable-temperature static susceptibilities for H_2(tbp)I and Ni(tbp)I (Figure S1 in Supporting Information) and the susceptibilities of H_2(tbp) (-3.25×10^{-4} emu mol^{-1}) and Ni(tbp) (-3.82×10^{-4} emu mol^{-1}) were measured for diamagnetic core correction. The correction for $^1/_3$ I_3^- is -1.15×10^{-4} emu mol^{-1} from Pascal's constant. The total diamagnetic correction for H_2(tbp)I and Ni(tbp)I is -4.40×10^{-4} and -4.97×10^{-4} emu mol^{-1}, respectively. The susceptibility for both samples remains almost constant from room temperature to 30 K, indicative of a metal-like, temperature-independent Pauli paramagnetism. Upon further cooling of the sample the susceptibility increases rapidly and can be fit approximately to an equation composed of a temperature-independent Pauli-paramagnetism term and a Curie−Weiss term,

(62) Kittel, C. In *Quantum Theory of Solids;* Wiley: New York, 1987; pp 237−248.
(63) Fukuyama, H.; Yoshida, K. *J. Phys. Soc. Jpn.* **1979**, *46*, 1522−1528.
(64) Kamimura, H.; Takemori, T.; Kurobe, A. *Anderson Localization;* Springer-Verlag: Berlin, 1982.

$$\chi_T = \chi_P + C(T - \Theta)^{-1} \quad (2)$$

where T is temperature, C (emu K mol^{-1}) is the Curie constant, and Θ (K) is the Weiss temperature.[65] The resultant values for χ_P (emu mol^{-1}), C, and Θ are as follows: H_2(tbp)I, 3.84×10^{-4}, 4.28×10^{-3}, and -4.13; Ni(tbp)I, 3.75×10^{-4}, 1.01×10^{-3}, and -0.33. The Curie constant represents the localized spins; these arise from localized conduction electrons and from localized spins in Cu^{II} $d_{x^2-y^2}$ orbitals. But since the amount of Cu(tbp)I impurity is small (<50 ppm), in the present instance the Curie constant measures the strength of localization. The larger Curie constant indicates that the conduction electrons are more localized in H_2(tbp)I than in Ni(tbp)I, probably owing to the larger amount of crystal defects or organic impurities. The result is consistent with the conductivity measurements that show H_2(tbp)I to have poorer conductivity than does Ni(tbp)I. The Weiss temperature can be analyzed in a similar way. The negative Weiss temperature indicates antiferromagnetic coupling among localized conduction electrons. The larger negative Weiss temperature for H_2(tbp)I once again demonstrates a larger number of localized electrons. The temperature-independent Pauli paramagnetism is almost identical for H_2(tbp)I and Ni(tbp)I. According to the one-dimensional tight-binding model, the transfer integral t (erg) is written as

$$t = N\beta^2[\chi_P \pi \sin(\pi\rho/2)]^{-1} \quad (3)$$

where N is Avogadro's number (6.022×10^{23} molecules mol^{-1}), β is the Bohr magneton (9.273×10^{-21} erg G^{-1}), and ρ is the degree of oxidation. From the values of χ_P above and $\rho = {}^1/_3$, we obtain bandwidths ($4t$) of 0.214 and 0.219 eV for H_2(tbp)I and Ni(tbp)I, respectively. These values are smaller than those for pure H_2(pc)I (0.296 eV) and Ni(pc)I (0.381 eV). There is no clear relationship, though, between the bandwidth and the strength of localization.

Electron Paramagnetic Resonance. A free radical signal ($g \sim 2$) is observed for unoxidized H_2(tbp) and Ni(tbp). The origin of a free radical signal in diamagnetic porphyrins has been the subject of several papers.[66−68] We confirm that the signal originates from trapped charge carriers at structural defects or impurity sites.[69] The much larger signal for the precursors H_2(tbp) and Ni(tbp) than for H_2(pc) and Ni(pc) suggests that tbp has more defects or impurities, and it is these that make H_2(tbp) and Ni(tbp)I less conducting than H_2(pc)I and Ni(pc)I at low temperatures.

Our earlier EPR study[44,45] of what we now know was impure Ni(tbp)I reported the following: (1) The powder EPR signal for Ni(tbp)I at room temperature showed a roughly symmetric line with the unusally large isotropic g value of $g_{av} = 2.024$. (2) g_{av} increased from 2.024 at 295 K to 2.062 at 77 K. (3) The peak-to-peak line width at room temperature, $\Gamma = 105$ G, was also unusually large. (4) The line width further increased from 105 G at 295 K to 320 G at 77 K. From these results we concluded that the [Ni(tbp)]$^+$ cation exhibited an electronic tautomerism with interconversion between [Ni^{III+}(tbp)] and [Ni^{II}(tbp)$^+$]. Thus, we believed Ni(tbp)I to be a doubly mixed-valence conductor, where conduction electrons were not only in the rings but also hopping into Ni orbitals at low temperatures. Similar results were seen for Ni(pc)$Y_{0.5}$, Y = SbF_6^- and AsF_6^-.[70] Our new samples of Ni(tbp)I, from which paramagnetic transition-ion impurities such as Cu(tbp) have been carefully excluded, give totally different results. Values of the $g_{||}$, $g_\perp$, $\Gamma_{||}$, and $\Gamma_\perp$, the parallel and perpendicular components of g and of the line width, as determined by computer simulation of the signals, are summarized in Table 3.

Table 3. Computer-Simulated EPR g Values and Line Widths for H_2(tbp)I and Ni(tbp)I

sample	T (K)	$g_\perp$	$g_{||}$	$\Gamma_\perp$ (MHz, G)	$\Gamma_{||}$ (MHz, G)
H_2(tbp)I	300	2.0026	2.0045	6, 2.1	15, 5.4
	77	2.0031	2.0059	8, 2.9	20, 7.1
	4.2	2.0012	2.0050	10, 3.6	25, 8.9
	1.9	2.0010	2.0044	10, 3.6	25, 8.9
Ni(tbp)I	300	2.0010	2.0070	10, 3.6	10, 3.6
	77	2.0020	2.0090	13, 4.6	13, 4.6
	4.2	2.0025	2.0140	15, 5.4	25, 8.9
	1.9	2.0025	2.0140	15, 5.4	25, 8.9

Both H_2(tbp)I and Ni(tbp)I show similar behavior. The g values are close to the free-electron value ($g = 2.0023$), are almost temperature-independent, and are similar to those values in H_2(pc)I and Ni(pc)I. The slightly larger value for $g_{||}$ than for $g_\perp$ results from back-electron-transfer of electron density from iodine to the ring. The line widths for H_2(tbp)I and Ni(tbp)I are extremely narrow at room temperature and increase only slightly as the temperature is lowered. The narrow line widths are typical for one-dimensional conductors because the direction of spin−lattice relaxation is restricted and slower. The slight increase in the line widths probably results from the presence of otherwise undetectably small amounts of paramagnetic impurities. In these systems the g values and line widths are described by the susceptibility-weighted average of those for the exchange-coupled conduction electrons, with temperature-independent susceptibility, and the Curie-like unpaired d electrons; thus the influence of the latter increase as the temperature is decreased. The unexceptional behavior of the EPR variables of the new materials and the absence of a significant differences between H_2(tbp)I, necessarily a ring-centered conductor, and Ni(tbp)I show that Ni(tbp)I is not a doubly mixed-valence conductor but rather is a simple ring-oxidized conductor with a diamagnetic Ni^{II} center and that the same is true for the M(pc)Y_x.[70]

Acknowledgment. We thank the National Science Foundation for funding (Grants DMR-9523228 (B.M.H.), CHE-8911215 (R.L.M.), and DMR-9632472 (the MRL Program at the Materials Research Center of Northwestern University (J.A.I., B.M.H.)). R.L.M. also thanks the the donors of the Petroleum Research fund of the American Chemical Society for partial funding (Grant 25966-B).

Supporting Information Available: Tables of positional and displacement parameters, calculated and observed diffuse amplitudes, bond distances and angles, and a metrical comparison of H_2(tbp)I and Ni(tbp)I and Figure S1, showing the temperature dependence of the magnetic susceptibility for H_2(tbp)I and Ni(tbp)I (5 pages). Ordering information is given on any current masthead page.

IC961490S

(65) For the purposes of this paper a more detailed analysis is not warranted. For example, the temperature-dependent part could be described by a term $dT^{-\gamma}$.

(66) Assour, J. M.; Harrison, S. E. *J. Phys. Chem.* **1964**, *68*, 872−876.
(67) Raynor, J. B.; Robson, M.; Torrens-Burton, A. S. M. *J. Chem. Soc.* **1977**, 2360−2364.
(68) Harbour, J. R.; Loufty, R. O. *J. Phys. Chem. Solids* **1982**, *43*, 513−520.
(69) Jerome, D.; Schultz, H. J. In *Studies in Physics;* 1982; pp 299−490.
(70) Yakushi, K.; Yamakado, H.; Yoshitake, M.; Kosugi, N.; Kuroda, H.; Sugano, T.; Kinoshita, M.; Kawamoto, A.; Tanaka, J. *Bull. Chem. Soc. Jpn.* **1989**, *62*, 687−696.